Ceramics International 49 (2023) 26900–26909

Contents lists available at ScienceDirect

Ceramics International

journal homepage: www.elsevier.com/locate/ceramint

TiO_2 nanostructures synthesized by electrochemical anodization in green protic ionic liquids for photoelectrochemical applications

G. Sánchez-García, E. Da Silva, R.M. Fernández-Domene, A. Cháfer, V. González-Alfaro, B. Solsona **, R. Sánchez-Tovar *

Departamento de Ingeniería Química, Universitat de València, Av de la Universitat, s/n, 46100, Burjassot, Spain

ARTICLE INFO

Handling Editor: Dr P. Vincenzini

Keywords:
TiO_2 nanostructures
Catalysts
Ionic liquid
Photoelectrochemical water splitting

ABSTRACT

This work studies the influence of the 2-hydroxyethylammonium acetate (2-HEAA) ionic liquid (IL) as an electrolyte in the electrochemical anodization of titanium for the synthesis of nanostructures for photoelectrochemical water splitting. Different 2-HEAA IL concentrations were used ranging from 0 to 4% v/v (IL-0 to IL-4) in electrolytes containing NH_4F, water and ethylene glycol. Morphological, structural and electrochemical characterization of the nanostructures was carried out by means of field emission scanning electron microscopy (FE-SEM), high resolution transmission electron microscopy (HRTEM), X-ray diffraction (XRD), electrochemical impedance spectroscopy (EIS), and Mott-Schottky (MS) analysis. Additionally, photoelectrochemical tests were carried out in order to evaluate the efficiency of these materials as catalysts for water splitting applications. According to the obtained results, the electrolyte used for electrochemical anodization should contain little amount of NH_4F (0.05 M) in order to obtain efficient nanostructures for photoelectrochemical purposes. However, small concentrations of IL (IL-0.25) resulted in nanostructures with higher photocurrents than doubling the NH_4F concentration to 0.1 M. Therefore, the IL addition contributes to a more sustainable electrolyte formulation. The best photoelectrochemical response for water splitting processes was obtained for the nanostructures anodized with 1% v/v of 2-HEAA IL (IL-1) due to their high surface/area (higher pore diameters, smaller nanotubes wall thickness and higher nanotubes lengths), better crystallinity and electrochemical response, showing photocurrents more than 100% higher than the ones obtained for the nanotubes anodized without IL.

1. Introduction

In the last few decades, the scientific community has focused on finding an alternative to fossil fuels in order to satisfy the growing energetic demand taking into consideration the need to reduce environmental pollution. Therefore, new technologies have been developed to generate energy from renewable sources.

One of the most promising technologies is the use of molecular hydrogen in fuel cells, since water is the only by-product. Recently, attention has been drawn to the photoelectrochemical splitting of water to produce hydrogen (and oxygen). This process takes place in a photoelectrochemical cell, in which one possible configuration could be a semiconductor (photoanode) and a counter electrode (cathode) immersed in an electrolyte [1,2]. When sunlight shines onto the semiconductor acting as a photocatalyst and applying a small polarization, electrons migrate from the valence band to the conduction band and electron-hole pairs are generated. The electrons reduce water into hydrogen at the cathode, while the holes at the photoanode/electrolyte interface take part in the water oxidation to oxygen [3,4].

Titanium dioxide has been stated as one of the most effective and useful materials for photoelectrocatalysis, due to its chemical and thermal stability, its appropriate morphological and optical properties and its low manufacture costs [5,6]. TiO_2 nanostructures can be synthesized in many ways, but the electrochemical anodization of titanium has become one of the most popular in the research field. The main reasons for this are the relatively low investment and operational costs and the possibility of obtaining different nanostructures with controlled/tailored morphology based on anodization parameters (anodization voltage, electrolyte, time …) [7,8].

As outlined above, these nanostructures have been synthesized with

* Corresponding author.
** Corresponding author.
E-mail addresses: benjamin.solsona@uv.es (B. Solsona), rita.sanchez@uv.es (R. Sánchez-Tovar).

https://doi.org/10.1016/j.ceramint.2023.05.227
Received 9 January 2023; Received in revised form 15 May 2023; Accepted 24 May 2023
Available online 1 June 2023

different morphologies, such as nanotubes, nanowires, nanopores, etc. Titanium dioxide nanotubes have gained increasing attention due to their high surface area to volume ratio, which has allowed to improve the photocatalytic activity of this material [9–11].

Taking all of this into account, investigation in this field has focused on experiment design in order to grow nanotubes with the best possible properties. For example, the composition of the electrolyte is one of the most determinant anodization parameters. The work of Assefpour-Dezfuly et al. (1984) [12] constitutes the first report on nanotubes or nanopores growth on titanium by electrochemical anodization using fluoride ions in the electrolyte Later, in 1999, this study was followed by Zwilling et al. [13] using hydrofluoric acid in the anodization solution for the formation of self-organized TiO_2 nanotubes. For the growth of nanotubes, organic based electrolytes are usually employed containing ethylene glycol or glycerol, water and fluorides, which can be present in different forms: NH_4F, HF, NaF … [8,14–17]. Nowadays, the use of ionic liquids for electrochemical anodization has been introduced in the synthesis of these nanostructures. Ionic liquids are highly conducting organic solvents, presenting important advantages compared to traditional solvents, such as high electrochemical stability and no volatility. These liquids can be classified into two categories, depending on composition and synthesis: protic and aprotic [18]. Protic ionic liquids (PILs) present a much simpler manufacture process and fewer operational costs than the aprotic ones. In addition, the protic group has a better toxicological profile and biodegradability [19,20].

In 2008, an ionic liquid was used for the first time in the electrochemical anodization of titanium: 1-butyl-3-methylimidazolium tetrafluoroborate [BMIM][BF_4] [21]. Later on, more research was made and conditions were improved, using the same ionic liquid but different anodization parameters [14,22–24]. In recent years, more ionic liquids have been tried for this purpose, such as 1-ethyl-3-methylimidazolium tetrafluoroborate [EMIM][BF_4], 3-methyl-1-octyimidazolium tetrafluoroborate [OMIM][BF_4] [25], 1-n-butylpyridinium chloride [BPy][Cl] [26], 1-n-butyl-3-methylimidazoly chloride [BMIM][Cl] [22] and ethylammonium nitrate [EAN][NO_3] [27]. However, studies have focused on the use of aprotic ionic liquids, whose synthesis is not environmentally friendly. Therefore, further research in the use of protic ionic liquids is a promising pathway, with the purpose of introducing PILs to grow nanotubes by electrochemical anodization reducing the use of fluorides, thus contributing to a more sustainable electrolyte formulation.

In the present work, we study the synthesis of self-organized TiO_2 nanotubes by the anodization of Ti in electrolytes composed of ethylene glycol (EG), water, ammonium fluoride, and the ionic liquid (2-hydroxyethyl)ammonium acetate, which is a protic ionic liquid. In particular, we investigate how different ionic liquid concentrations influence the morphology, structure, electrochemical and photoelectrocatalytic activity of the TiO_2 nanotubes formed by electrochemical anodization.

2. Experimental

Titanium foil (1 × 1 cm) was ultrasonically washed in acetone, ethanol and deionized water for 5 min for each solvent and then dried in a nitrogen stream. Anodization took place in a two-electrode electrochemical cell, where the titanium foil was used as the working electrode and Ag/AgCl (3 M KCl) as the reference electrode. The electrolyte used was composed of ethylene glycol, EG, (98% v/v), ammonium fluoride (0.05 M NH_4F), deionized water (1 M), and the ionic liquid 2-HEAA IL (0.25, 0.50, 1.0, 2.0 and 4.0% v/v, named as IL-0.25, IL-0.5, IL-1, IL-2 and IL-4). The different samples (with an exposed area to the electrolyte of 0.5 cm^2) were anodized for 30 min under a voltage of 55V. After each test, anodized films were washed with ethanol and deionized water and then dried with a N_2 stream. The last step to obtain a non-amorphous structure was the annealing of the films in air at 450 °C for 1h.

We must remark that the ionic liquid (2-HEAA IL) was synthesized at the laboratory following the method reported elsewhere [28,29]. The characterization undertaken to check the method of synthesis and the purity of the IL was made by Fourier transform infrared (FTIR) spectroscopy and carbon nuclear magnetic resonance spectrum (RMN). The results are shown in Figs. S1 and S2. The spectra obtained agree with that expected for this ionic liquid [30].

The dynamic viscosity of the different electrolytes used during the experiments was measured by a viscometer (DV-II. Brookfield Engineering Laboratory, U.S). Conductivity measurements were also carried out using a conductivity meter.

The morphology of the nanotubes was studied by the technique of field-emission scanning electron microscopy (FESEM), collecting images at an operation voltage of 5 kV with a Hitachi S4800 microscope, and by high resolution transmission electron microscopy (HRTEM) using a FEI Tecnai G2 F20 TWIN with an operation voltage of 200 kV.

To confirm the crystalline structure of TiO_2 formed in the films X-ray diffraction (XRD) patterns were collected using a Philips X'Pert diffractometer equipped with a graphite monochromator operating at 40 kV and 30 mA, and employing nickel-filtered CuKα radiation (λ = 0.1542 nm).

Additionally, band gap values of the different nanostructures were calculated, by means of the Tauc plot, from UV–Vis absorbance measurements using a spectrophotometer (Shimadzu) in the wavelength range of 200–800 nm.

The electrochemical and photoelectrochemical water splitting tests were carried out in a three-electrode cell, connected to a potentiostat (Palmsens4). The TiO_2 nanostructure was placed as the working electrode and only 0.5 cm^2 of it was exposed to the test solution. A platinum tip was used as the counter electrode and a saturated Ag/AgCl (3 M KCl) as the reference electrode.

For both electrochemical and photoelectrochemical measurements, 1 M KOH was used as the electrolyte solution. Electrochemical impedance spectroscopy experiments were performed at 0.5 $V_{Ag/AgCl}$ using an amplitude of 0.01 V and scanning frequencies from 100 kHz to 0.01 Hz, while Mott-Schottky plots were carried out at a 5000 Hz frequency, scanning the potential from 0.5 to −1 $V_{Ag/AgCl}$.

The photoelectrochemical water splitting tests took place under UV light (λ = 365 nm) provided by a LedControl UV LED (Opystec Dr. Gröbel, Germany) at a power of 100 mW/cm^2. Photocurrent density vs. applied potential was recorded by chopped light irradiation (60 mA in the dark and 20 mA in the light), while scanning the potential from −0.4 V to +0.54 V with a scan rate of 5 mV/s.

3. Results and discussion

3.1. Physicochemical properties of electrolytes

Dynamic viscosity and conductivity of the electrolytes used in the formation of the nanotubes, composed of ethylene glycol, water and NH_4F, and different amounts of 2-HEAA were determined. These properties affect the morphology of the nanostructures, since the diffusion and mobility of the ionic species to the anode and further penetration

Table 1
Dynamic viscosity and conductivity of pure 2-HEAA and of electrolytes used in TiO_2 nanostructures synthesis.

Sample[a]	Viscosity (mPa·s)	Conductivity (μS/cm)
IL-0	10.20	353.7
IL-0.25	7.68	455.3
IL-0.5	7.68	513.7
IL-1	8.96	666.7
IL-2	7.68	989.7
IL-4	15.40	1439.7
2-HEAA	286.70	340.0

[a] Electrolyte composed of ethylene glycol, water 1 M, NH_4F 0.05 M and 2-HEAA (expressed in % v/v).

through the oxide layer, depend on them [25,26]. Table 1 shows the results corresponding to the different electrolytes.

According to Tables 1 and it is clear that for the electrolytes with 2-HEAA concentrations between 0.25% and 2%, viscosities are similar to each other but lower than the electrolyte without ionic liquid. This decrease can be explained by the rupture of cation-cation, anion-anion and cation-anion bonds due to the weakening of electrostatic and Van deer Waals interactions between the 2-HEAA ions [27]. On the other hand, when the amount of ionic liquid is increased up to 4%, there is a significant rise in the viscosity of the electrolyte. This behavior is due to the strong effect of the elevated viscosity of the ionic liquid, which prevails over the ionic interactions. Moreover, a coordination complex may be formed between the acetate of the ionic liquid and titanium, since the formation of a Ti-acetate complex has been reported before [31].

Furthermore, the conductivity of the electrolyte increases with increasing 2-HEAA concentration. As the presence of ions grows, it is easier to conduct electric current. However, for the pure ionic liquid the conductivity significantly drops due to the low ion mobility because of its very high viscosity [32,33].

3.2. Electrochemical anodization of titanium

Fig. 1 shows the current density registration during the electrochemical anodization of titanium foil at 55V, representing the balance between the rate of titanium oxide formation by the application of a potential, and the rate of its dissolution due to the presence of fluoride ions in the electrolyte. It is possible to appreciate the three typical stages of nanotube growth in all curves except in the one corresponding to 4% v/v 2-HEAA electrolyte (IL-4).

As can be observed in Fig. 1, first, the current density abruptly drops as a consequence of the formation of a compact titanium oxide layer. Later, fluoride ions begin to attack the oxide layer, forming the soluble complex $[TiF_6]^{2-}$ (Eq. (1)) as the same time as random and irregular nanopores begin to appear on the layer. This phenomenon corresponds to a slight increase in the current density curve, known as the second stage.

$$TiO_2 + 6F^- + 4H^+ \rightarrow [TiF_6]^{2-} + 2H_2O \quad (1)$$

In the final stage, current density distributes evenly between the pores, which leads to the regular growth of nanotubes. This means that the formation of titanium dioxide is faster than its dissolution by the fluoride ions. In Fig. 1, this is represented by a slight decrease in current density at first, and by the stabilization of the curve to end. At this point, the rate of formation and dissolution of the oxide are almost the same, and nanotubes grow in length until the end of the anodization.

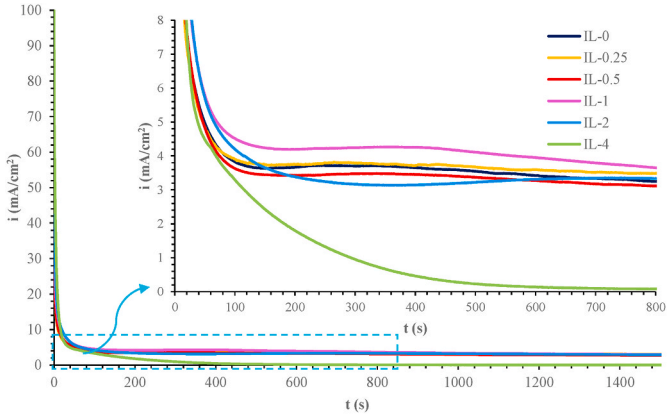

Fig. 1. Current density curves recorded during electrochemical anodization at 55V using an EG, 1 M H_2O, 0.05 M NH_4F electrolyte with different concentrations of 2-HEAA (% v/v).

It is clear that the registered curves in Fig. 1 are smooth and present no important fluctuations. This means that the organic nature of the electrolyte helps to achieve moderate oxidation and chemical dissolution rates [34]. Additionally, neither the current density nor the rate of nanotube growth present significant differences when comparing the curves of IL-0, IL-0.25 and IL-0.5. On the other hand, the higher current densities registered when anodization was carried out in IL-1 might be related to higher reaction rate in all the anodization stages.

When IL-2 was used for electrochemical anodization, stage II of nanotube growth occurs later in time, which means that the nanostructures are formed more slowly. This behavior can be explained by the organic contribution (bigger size of the molecules presented in the electrolyte due to its higher concentration in ionic liquid), leading to steric hindrance in the interaction between fluoride ions and the oxide layer.

Observing the curve corresponding to the IL-4, it is clear that only a compact oxide layer grows, and no nanotubes are formed, since the current density drops at the beginning of the process until it reaches a minimum and the system stabilizes. Once again, the difficulty of the interaction between the fluoride ions and the oxide layer caused by steric hindrance explains this phenomenon, as well as by the high viscosity of the solution which makes it more difficult for the species to diffuse through the electrolyte [8,33,35].

3.3. Morphological characterization of the photoelectrocatalysts

To determine the influence that (2-hydroxyethyl) ammonium acetate exerts on the structure and morphology of the anodized samples, FE-SEM images were obtained (Fig. 2 and S3).

On the one hand, images corresponding to IL-0 to IL-2 (Fig. 2a–e and S3a-e) confirm the growth of titanium dioxide nanotubes. On the other hand, Fig. 2f (IL-4) reveals the formation of a compact metal oxide layer, and no nanostructures whatsoever. Nanotubes cannot be formed since the high viscosity hinders the ion mobility through the solution and

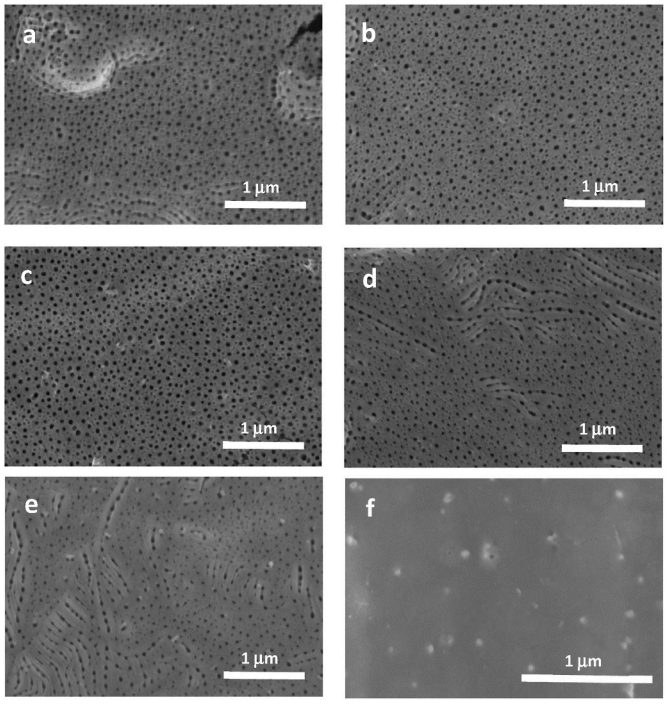

Fig. 2. FE-SEM top images of the titanium dioxide nanostructures synthesized by titanium electrochemical anodization with EG, H_2O 1 M, NH_4F 0.05 M and different 2-HEAA IL concentrations: (a) IL-0, (b) IL-0.25, (c) IL-0.5, (d) IL-1, (e) IL-2, (f) IL-4.

makes it difficult for the soluble complex $[TiF_6]^{2-}$ to form [7,36].

From these images (Fig. 2 and S3) it has been possible to determine the number of pores per surface unit of the initiation layer formed in the top of the nanotubes, as well as their diameters and length (Table 2).

No significant variation in pore density until the electrolyte reaches a concentration of 2-HEAA higher than 1% can be observed in Table 2. This agrees with the anodization curves presented in Fig. 1. Once the concentration of ionic liquid gets higher than 1%, the number of pores greatly decreases until they disappear. This phenomenon is related to the rate of the oxide layer formation being faster than the rate of its dissolution, and so the initiation layer prevails over the nanotube growth. Samples with the highest pore density are IL-0.5 and IL-1, which might be related to a better photoelectrocatalytic behavior.

In addition, for concentrations below 1% v/v of 2-HEAA, the pore diameters increase as the amount of ionic liquid in the electrolyte gets higher, growing from 38 ± 2 nm at IL-0 to 43 ± 4 nm at IL-1. In the same way, nanotubes get longer as the electrolyte becomes more concentrated in 2-HEAA, reaching their highest length for IL-1 (5.6 ± 0.6 μm). An increase in pore diameter together to higher nanotubes lengths enhances the catalytic surface of the samples. Thus, more light absorption could be harvested and, therefore, a better photoelectrocatalytic performance might be achieved [33].

According to the results, a higher concentration of ionic liquid (up to 1% v/v) increases the conductivity of the electrolyte, which facilitates mobility of reagents to the oxide surface and the dissolution of the initiation layer previously formed, therefore increasing diameters of the pores and nanotubes lengths. However, higher concentrations of IL (IL-2 and IL-4) obstruct the access of fluorides to the metal oxide layer, therefore, hindering nanotubes formation [33].

A detailed TEM study was undertaken to complement the data obtained by FESEM in order to get further insights into the morphological properties of the samples. As expected, the crystalline phase identified was for all the cases anatase TiO_2 (Fig. S4). Some representative TEM images of the ionic liquid (IL) modified TiO_2 nanostructures are shown in Fig. 3. These images have been taken using pieces of the nanostructures obtained by scratching the surface of the samples, which is the part affected by the anodization treatment (the active oxidized material).

In the case of the reference sample (that not treated with IL) a clear nanotubular morphology is observed. These tubes present an outer diameter of 80–100 nm with a thickness of the walls of 20–30 nm. In agreement with that observed by FESEM these nanotubes are packed together forming compact structures.

The treatment with low concentrations of IL (IL-0.25) did not lead to a change of the morphology but a clear variation in the nanotube dimensions. Then, the outer diameter of the nanotubes increases until 100–130 nm whereas the wall thickness clearly diminishes until 10–20 nm. A second effect caused by the treatment with ionic liquid is the generation of certain microporosity.

A further increase in the IL concentration (IL-1) meant just subtle differences but following a similar trend, i.e., wider tubes (110–140 nm) and thin walls (10–20 nm). Finally, the sample treated with the highest concentration of IL (IL-4) presented a completely different morphology compared to the other samples. Thus, the presence of nanotubes is scarce, the main part of the sample consisting in aggregated particles with undefined shapes. A deeper analysis of this sample allows us to find some small tubes. Interestingly, the tubes are remarkably tinier than those of the other samples, with outer diameters of 25–45 nm and wall thicknesses of 8–15 nm.

Table 2
Pore density, pore diameter and nanotubes length of the nanostructures anodized in EG, 1 M H_2O, 0.05 M NH_4F and different 2-HEAA IL concentrations.

Sample	Pore density (n°/μm^2)	Pore diameter (nm)	Nanotubes length (μm)
IL-0	73.89	38	4.7
IL-0.25	71.80	40	4.7
IL-0.5	82.63	42	4.8
IL-1	83.78	43	5.6
IL-2	44.74	32	5.2
IL-4	–	–	–

3.4. Structural characterization of the photoelectrocatalysts

After electrochemical anodization, samples were annealed, the XRD patterns of the different samples are shown in Fig. 4.

The diffraction peaks observed at 2θ = 25.2 and 48.1°, can be assigned to the TiO_2 anatase phase, specifically to the crystallographic planes of (101) and (200) [33,37]. The rest of peaks correspond to titanium (2θ = 38.2, 40.9,53.9, 62.2, 70.9 and 76.2°).

Fig. 4 shows how the crystallinity of the anatase phase varies depending on the amount of ionic liquid used during the titanium anodization. Taking as a reference the main peak of the anatase phase (101), it is clear that the intensity of this peak decreases when the nanostructure is prepared with a 2% v/v 2-HEAA electrolyte, and even disappears when the concentration rises up to 4%. A similar behavior is observed with the peak corresponding to the (200) plane, which is not totally formed for ionic liquid concentrations above 1% v/v.

Furthermore, crystallite size is a very important parameter in photocatalytic properties of metal oxides. Average crystallite size of nanotubes was estimated on the basis of the Scherrer equation [38], and the results are shown in Table 3.

Results from Table 3 reveal that nanostructures synthesized with ionic liquid content below 2% present very similar crystallite size, unlike the IL-4 nanostructure in which this parameter significantly increases. A smaller crystallite size is beneficial for the photocatalytic processes yield, since the transfer of charge carriers to the catalyst surface is improved and the chances of recombination decrease [39–41]. Therefore, it is expected that electrolytes with less than 2% v/v of 2-HEAA will provide nanostructures with better photocatalytic properties.

3.5. Electrochemical and photoelectrochemical characterization of the photoelectrocatalysts

Fig. 5a shows the experimental Nyquist plot for the TiO_2 nanostructures formed with different electrolytes, measured in 1 M KOH solution at a 0.5 $V_{Ag/AgCl}$ potential.

Fig. 5a shows that the impedance resistances decrease when increasing the IL concentration. According to the literature [42,43], EIS experimental data of TiO_2 nanostructures can be fitted to an electrical equivalent circuit made up of two RC time constants associated in series (Fig. 5b). In this circuit, constant phase elements (CPE) have been used instead of pure capacitors to account for the non-ideality of the system [44,45].

Rs stands for the electrolyte resistance, while the time constants R_1CPE_1 and R_2CPE_2 are related to the TiO_2 nanotubular structure and to the compact TiO_2 underlayer, respectively. After the fitting to the equivalent circuit, the obtained results are presented in Table 4. Chi-squared (χ^2) values were used to evaluate the quality of data fitting to the proposed equivalent circuit. χ^2 values were of a magnitude order of 10^{-3} or lower indicating the suitability of the circuit. This is also shown in Fig. 5a, where the simulated data are shown as solid lines.

Table 4 shows similar *Rs* values regardless of the ionic liquid concentration, since the same electrolyte was used in all tests. When referring to the porous layer resistance (R_1), samples IL-0.5 and IL-1 show lower values compared to the nanostructure synthesized without ionic liquid (IL-0), which can be related to their higher porosity and surface area (see Table 2). Hence, it can be inferred that adding 2-HEAA to the anodization solution benefits the electron transfer and hole diffusion and this would result in a better photoelectrochemical performance. For more concentrated electrolytes (IL-2) R_1 abruptly drops, which may be linked to an excess number of defects, as will be discussed below.

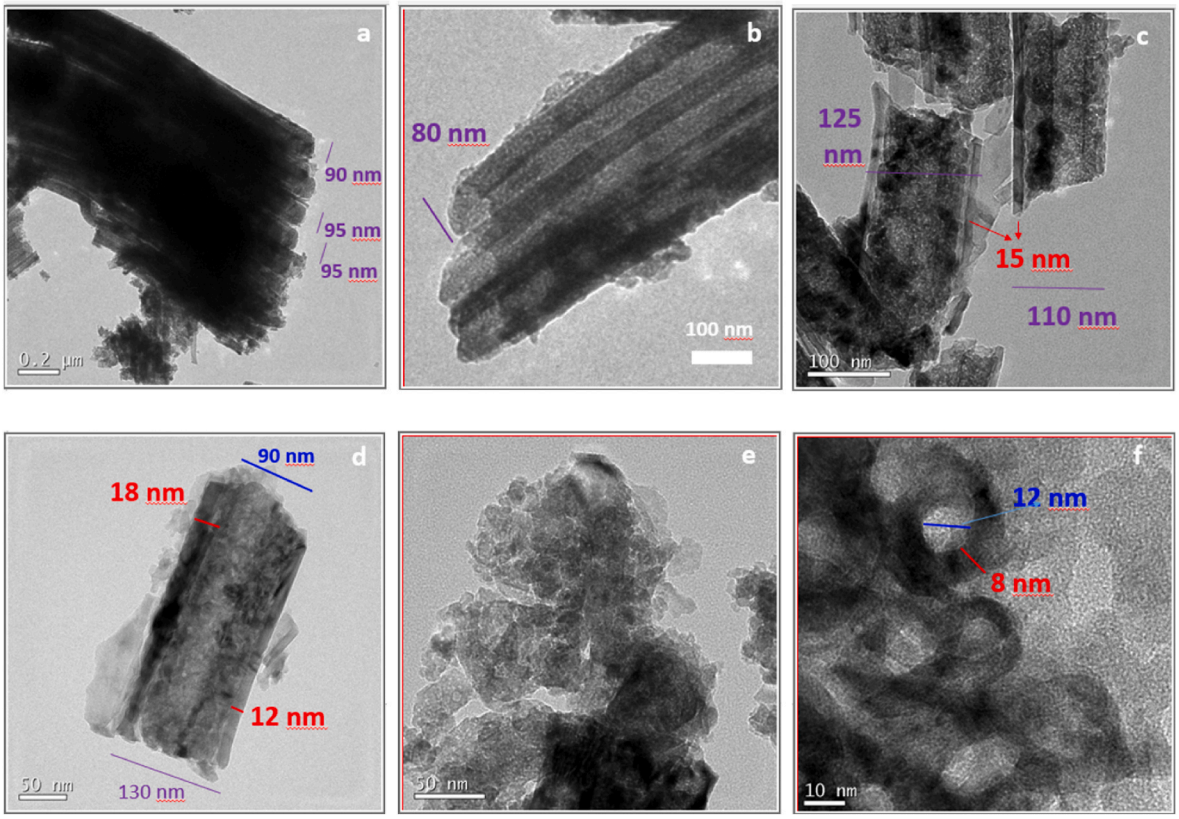

Fig. 3. TEM images of the ionic liquid modified TiO_2 nanostructures: LI-0 (a and b), LI-0.25 (c), LI-1 (d), LI-4 (e and f).

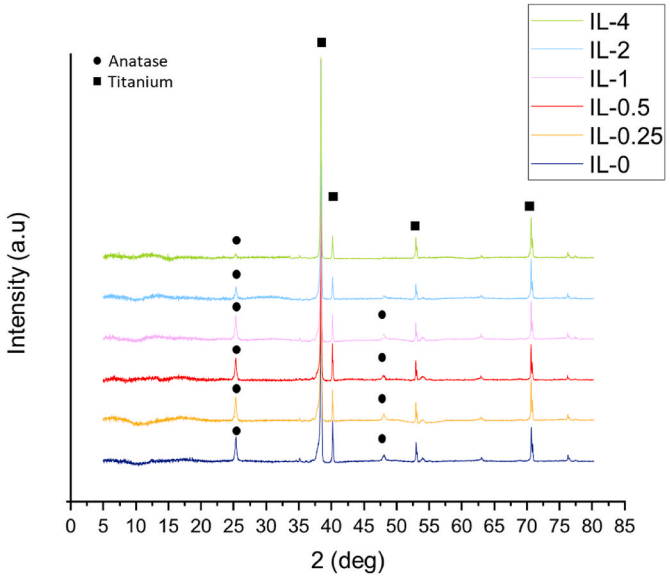

Fig. 4. XRD patterns of TiO_2 nanostructures after anodization at 55V in the electrolyte composed of EG, H_2O, NH_4F, and different amounts of 2-HEAA IL.

It should be noticed that *R1* value for IL-4 sample is not shown in Table 4, since the morphology of this nanostructure consisted of a compact TiO_2 layer, so, data were adjusted to an equivalent circuit of one time constant.

Table 4 also shows that R_2 values are much bigger than R_1, since they correspond to the compact titanium dioxide layer.

Table 3
Crystallite size of nanotubes synthesized by titanium electrochemical anodization using EG, 1 M H_2O, 0.05 M NH_4F and different 2-HEAA concentrations.

Sample	Crystallite size (nm)
IL-0	21.28
IL-0.25	22.21
IL-0.5	22.31
IL-1	23.49
IL-2	23.93
IL-4	30.44

3.6. Mott-Schottky analysis

Mott-Schottky plots were carried out at a frequency of 5 kHz for the titanium dioxide formed in different ionic liquid concentration electrolytes, measured in a 1 M KOH solution and scanning the potential from 0.5 to −1 $V_{Ag/AgCl}$. Results are shown in Fig. 6.

The positive slopes of the MS plots shown in Fig. 6 reveal that the synthesized TiO_2 nanostructures are n-type semiconductors, electrons being the dominant charge carriers.

Mott-Schottky plots allow to calculate the flat band potential (E_{FB}) and the donor density (N_D) using Eq. (2) [46]:

$$\frac{1}{C^2} \approx \frac{1}{{C_H}^2} + \frac{1}{{C_{SC}}^2} = \frac{1}{{C_H}^2} + \frac{2}{e \cdot \varepsilon_T \cdot \varepsilon_0 \cdot N_D} \cdot \left(E - E_{FB} - \frac{k \cdot T}{e} \right) \quad (2)$$

where C_{SC} is the space charge layer capacitance, C_H is the Helmholtz layer capacitance, e the electron charge ($1.60 \cdot 10^{-19}$ C), ϵ_0 the vacuum permittivity ($8.85 \cdot 10^{-14}$ F/cm), ϵ the relative dielectric constant of TiO_2 (100 [47]), E the applied potential, k the Boltzmann constant ($1.38 \cdot 10^{-23}$ J/K) and T the absolute temperature [46].

Table 5 shows the calculated E_{FB} and N_D for all titanium dioxide

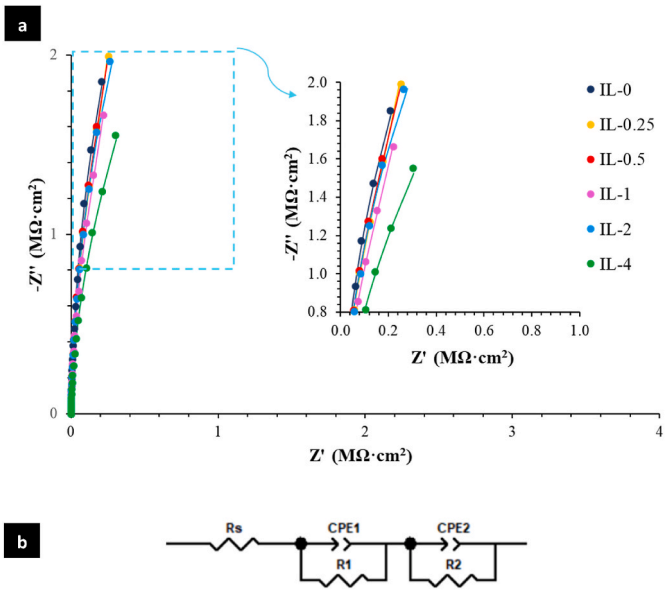

Fig. 5. (a) Experimental Nyquist of the EIS data, (b) Electrical equivalent circuit used to simulate experimental EIS data.

Table 4
Resistances obtained by fitting EIS data to the equivalent circuit of Fig. 5b.

Sample	*Rs* (Ω·cm^2)	R_1 (Ω·cm^2)	R_2 (Ω·cm^2)·10^6
IL-0	2.42	23.80	1.76
IL-0.25	2.37	20.39	1.65
IL-0.5	2.32	15.16	1.24
IL-1	2.31	16.04	1.32
IL-2	2.34	7.46	1.16
IL-4	2.42	–	0.94

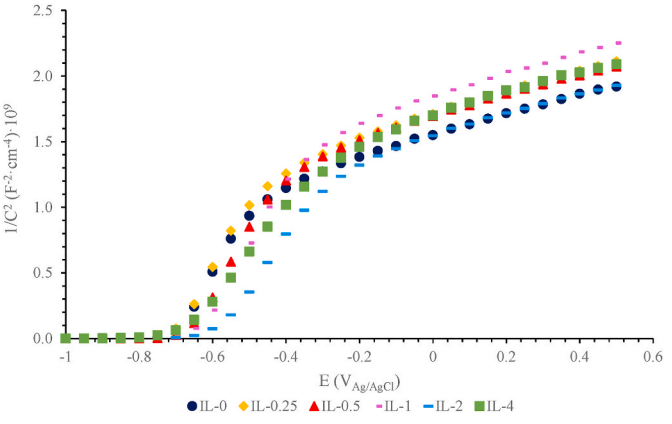

Fig. 6. Mott-Schottky plots obtained at a frequency of 5 kHz for TiO_2 nanostructures formed with electrolyte containing different concentrations of 2-HEAA.

nanostructures.

The donor density is related to the defects of the nanostructures, for titanium dioxide being, the oxygen vacancies the dominant defects [48]. For ionic liquid concentrations below 1% v/v, all nanostructures present similar donor densities, while for greater IL concentrations (IL-2 and IL-4) N_D increases as the electrolyte gets more concentrated in 2-HEAA. This result is in accordance with EIS and XRD data, since IL-2 and IL-4 showed the lowest R_1 values and the lowest degree of crystallinity.

The increase in donor density can have a positive effect on the photoelectrocatalytic behavior, since this fact increases the electrical conductivity of titanium dioxide. However, oxygen vacancies can act as recombination centers for electrons and holes, which involves a decrease in their contribution to the photoelectrochemical process as they become trapped [49,50].

Table 5
Flat band potential and charge donor density for TiO_2 nanostructures synthesized by electrochemical anodization in electrolytes with EG, 1 M H_2O, 0.05 M NH_4F and different 2-HEAA IL concentrations.

Sample	E_{FB} ($V_{Ag/AgCl}$)	N_D (cm^{-3})·10^{19}
IL-0	−0.72	5.64
IL-0.25	−0.72	5.17
IL-0.5	−0.68	5.19
IL-1	−0.70	4.95
IL-2	−0.61	6.62
IL-4	−0.69	6.71

The flat band potential is the potential at which the semiconductor Fermi level is equal to the redox potential of the solution. In other words, it is the potential that must be applied in the semiconductor/electrolyte interface for the energy bands to remain flat. From Tables 5 and it can be inferred that adding ionic liquid to the electrolyte has no significant effect on the flat band potential, since values hardly vary.

3.7. Band gap measurements by ultraviolet–visible spectroscopy

The band gap values (Table 6) of the different nanostructures were calculated using UV–visible spectroscopy and adjusting data to Tauc equation (Fig. S5). We must mention that the energy band gaps have been directly determined using the classical approach through the Tauc Plot. Unfortunately, in the cases where the absorbance below the band gap is not negligible (as in our study) the values for the band gaps present certain inaccuracy [51]. However, although, the approach followed in the present article shows some error and must be taken with caution, the values found suggest a defined trend.

According to Table 6, the use of ionic liquid decreases the band gap value compared to the preparation without IL. This trend occurs until reaching the concentration of 2%, the value for IL-1 being the lowest, and all being below the band gap of anatase crystalline TiO_2 (~3.2 eV, according to the literature [48,52]). The narrowing of the band gap of a photoelectrocatalyst means the expansion of the range of wavelengths of the solar spectrum which could generate electron-hole pairs. Consequently, an increase in the photoelectro-activity of the nanostructures takes place [53,54].

The sample prepared with the highest concentration of ionic liquid, IL-4, presents the highest band gap value, which is even higher than that of the reference sample (IL-0). This wide band gap limits the use of these nanostructures for photoelectrochemical applications with solar light.

3.8. Photoelectrochemical water-splitting measurements

Fig. 7 shows the photoelectrochemical water splitting performance under UV-light conditions (λ = 365 nm) for the different nanostructures (Fig. 7a) and the photocurrent densities at 0$V_{Ag/AgCl}$ vs the ionic liquid

Table 6
Band gap values (in eV) of the nanostructures synthesized by electrochemical anodization in electrolytes with EG, 1 M H_2O, 0.05 M NH_4F and different 2-HEAA IL concentrations.

Sample	Band gap (eV)
IL-0	3.25
IL-0.25	3.18
IL-0.5	3.18
IL-1	3.17
IL-2	3.19
IL-4	3.48

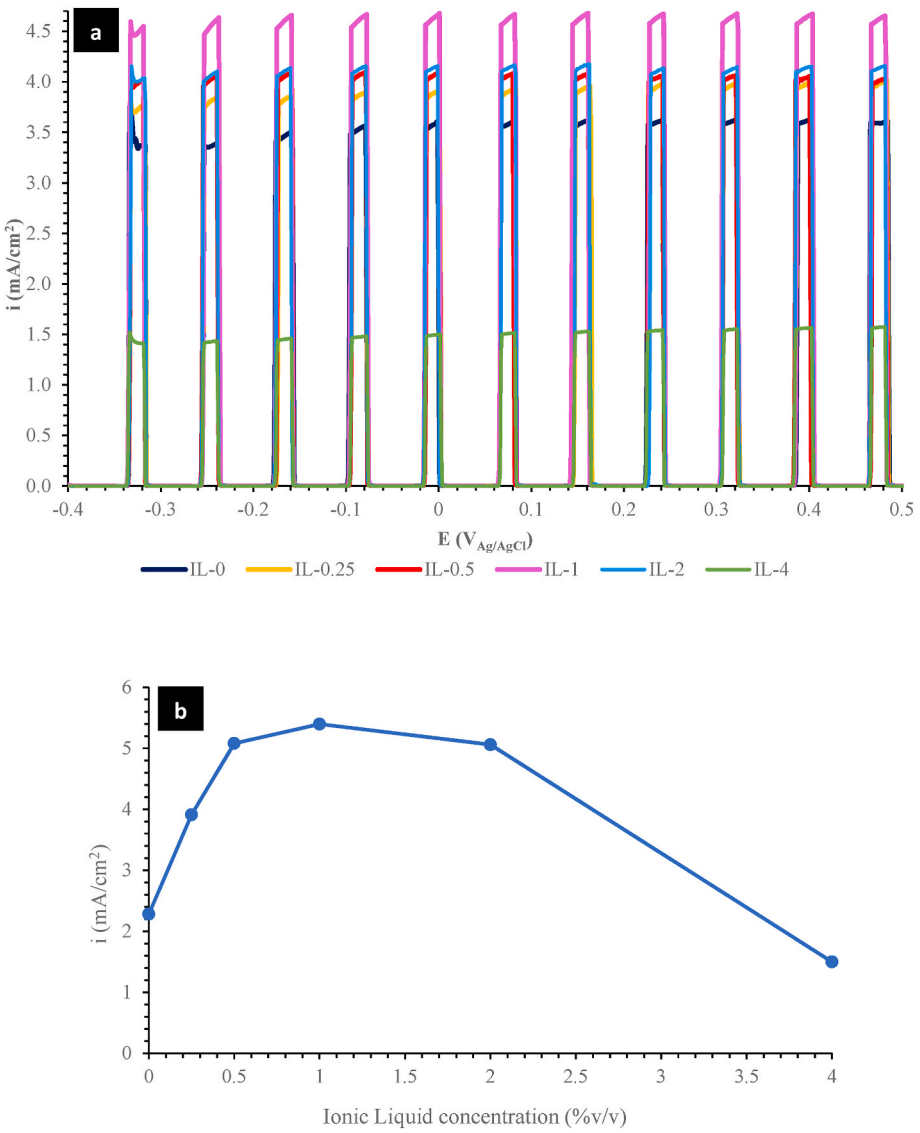

Fig. 7. (a) Photocurrent transient vs. potential for the TiO_2 nanostructures formed using an EG, 1 M H_2O, 0.05 M NH_4F electrolytes with different concentrations of 2-HEAA IL under UV-light ($\lambda = 365$ nm), (b) photocurrent density generated at 0V by samples synthesized in EG, 1 M H_2O, 0.05 M NH_4F electrolytes with different 2-HEAA IL concentrations.

concentration (Fig. 7b). Photocurrent vs potential curves were carried in order to see which of the photocatalysts present the best photoresponse for photoelectrochemical water splitting tests, which is achieved when the maximum photocurrents (with low and stable dark current density values) are obtained.

Fig. 7a shows that, in all cases, high anodic photocurrent densities are reached even at low potentials (see Fig. S6 where photocurrent densities reached saturation values at anodic potentials as negative as $-0.5V_{Ag/AgCl}$), which is useful for photoelectrochemical applications, since the maximum current density can be achieved by applying low polarization.

According to Fig. 7, it can be concluded that adding ionic liquid has a positive impact on the photoelectrocatalytic behavior of TiO_2 nanostructures, since the water splitting performances of samples IL-0.25 to IL-2 improve when compared to the reference electrolyte (IL-0). However, the addition of an excess of 2-HEAA IL (IL-4) has a negative effect on the photoelectrochemical response, showing photocurrent density values lower than those obtained for IL-0.

The nanostructure which presents the best photoelectrocatalytic behavior is the sample synthesized with 1% of 2-HEAA electrolyte (IL-1). This result is in well agreement with the morphological, structural and electrochemical characterization, where this nanostructure presented the largest and longest nanopores, smallest wall thickness, high crystallinity and crystallite size and a smaller, though enough, number of oxygen vacancies. On the other hand, the IL-4 sample is the nanostructure with the worst photoelectrocatalytic behavior, since the structure and electrochemical characterization showed the formation of a compact oxide layer, with almost no crystallinity, lowest surface area and many defects.

Fig. 7b shows the trend followed by the photocurrent density generated by the synthesized nanostructures, the sample IL-1 being the best photoelectrocatalyst for water splitting, since the photocurrent is increased 137% in comparison to IL-0.

Further experiments were carried out doubling the NH_4F content (from 0.05 M to 0.1 M) and in the absence of NH_4F (Fig. 8).

Fig. 8a compares the photocurrents for photoelectrochemical water splitting of the nanostructures anodized with 0.05 M and 0.1 M NH_4F without ionic liquid (0.1 M IL-0 and IL-0, respectively). Higher photocurrents were obtained for the 0.1 M IL-0 catalyst, since more and larger nanopores (56 nm vs. 43 nm diameters) are formed, comparing Fig. 8b

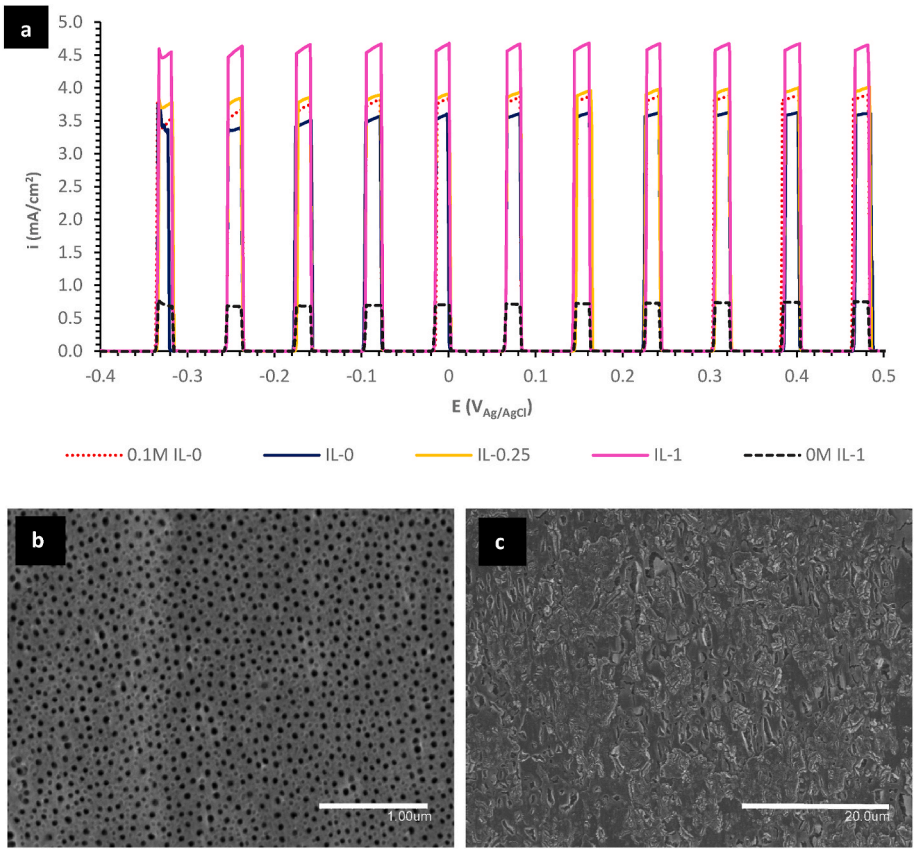

Fig. 8. (a) Photocurrent transient vs. potential curves for the TiO_2 nanostructures formed using EG, 1 M H_2O electrolytes with different concentrations of NH_4F and 2-HEAA IL under UV-light (λ = 365 nm); (b,c) FESEM images for (b) 0.1 M NH_4F IL-0 and (c) 0 M NH_4F IL-1.

with Fig. 2a. However, just by adding a little amount of 2-HEAA (IL-0.25) to the 0.05 M NH_4F electrolyte, the photoelectrocatalytic properties are slightly improved in comparison to the 0.1 M IL-0. These properties get even better when the ionic liquid concentration rises to 1% (IL-1), as photocurrent density increases more than 100% with respect to the sample labelled as 0.1 M IL-0. Considering the need to replace or reduce ammonium fluoride content in order to formulate a more sustainable electrolyte, the process can be doubly improved by using electrolytes with less NH_4F and more 2-HEAA, since it will be more environmentally friendly and the synthesized nanostructures will present a better photoelectrocatalytic performance.

On the other hand, Fig. 8a also shows that, in order to have competitive nanostructures for water splitting applications, it is necessary to use, not only a certain amount of IL (1% to have the better photoresponse), but also some amount of NH_4F, since samples anodized without NH_4F in the electrolyte but with IL concentration of 1% shows the formation of a heterogeneous compact TiO_2 layer. That is, by anodizing without fluorides no localize attack of the oxide layer occurs and neither nanopores nor nanotubes are formed (Fig. 8c). In fact, Fig. 8a shows that the photocurrent is reduced in more than 75% for the catalyst anodized without NH_4F (0 M IL-1) in comparison to the catalyst anodized in electrolytes with 0.05 M NH_4F (IL-0).

Further experiments were carried out to verify if by increasing the ionic liquid concentration it was possible to form homogeneous nanotube layers or if it was necessary to incorporate small amounts of NH_4F to the electrolyte in order to obtain competitive photocurrent densities for photoelectrochemical water splitting.

Fig. S7 (a to c) shows the morphology of the samples anodized without NH_4F and with an increasing amount of IL from 10 to 50% v/v (IL-10, IL 20 and IL-50) obtained by means of FE-SEM. In all cases, the morphology of the nanostructure is characterized by a very thin heterogeneous compact layer which is detached in same regions. According to the morphology of the samples presented in FE-SEM images, Fig. S7d shows the current densities vs time registers during anodization of the IL-10, IL-20 and IL-50 nanostructures, which are the typical curves of a compact layer formation. That is, current density decreases with time, firstly abruptly and then, they stabilize. In fact, Fig. 2Se shows the photoelectrochemical water splitting tests for the IL-10, IL-20 and IL-50 samples, presenting photocurrents, in the best case, 80% lower in comparison to the IL-0 nanostructure (without IL and with 0.05 M NH_4F).

4. Conclusions

In this work, we demonstrated that the addition of (2-hydroxyethyl) ammonium acetate to the traditionally used organic electrolyte composed of ethylene glycol, water and NH_4F allows the growth of nanotubes with different morphological parameters and has a big impact on their photoelectrocatalytic performance.

Using IL concentrations lower than 2% v/v, the addition of 2-HEAA improves the conductivity of the electrolyte, which accelerates the growth rate of the nanostructures. FE-SEM and HR-TEM images revealed that with the electrolyte IL-1, maximum surface area nanotubes were obtained with the bigger diameters and length together with the thinner wall thickness. For higher IL concentrations (IL-2 and IL-4), the number of nanopores decreased, as well as getting smaller and shorter until, eventually, disappearing.

XRD patterns show the presence of the TiO_2 anatase crystalline phase after annealing at 450 °C for 1h. Sample crystallinity decreases for the IL-2, where the main anatase peak (101) gets smaller and disappears at IL-4.

According to the electrochemical properties, EIS measurements show

that electrochemical resistances of the nanotubular layer decrease by increasing the IL concentration. On the other hand, MS plots show an n-type semiconductor behavior of the catalysts with an important increase in the number of defects for electrolytes with IL concentrations higher than 2% v/v, which may act as traps increasing the recombination of the electron and hole pairs. Additionally, the band gap value considerably increases for the IL-4 sample. Regarding to the photoelectrochemical water splitting tests the optimum catalyst was the IL-1, presenting photocurrents more than 100% higher than that obtained for the IL-0 sample and showing better photoelectrochemical response than doubling the NH_4F concentration in the electrolyte. Therefore, in this work, a new approach is presented for a sustainable electrolyte formulation.

Results obtained in this work also confirmed the need of using not only a certain amount of IL (1% v/v for the best of our catalysts) in the electrolyte to have competitive results for photoelectrochemical water splitting applications but also a low NH_4F content (0.05 M).

Declaration of competing interest

The authors declare that they have no known competing financial interests or personal relationships that could have appeared to influence the work reported in this paper.

Acknowledgments

Authors would like to acknowledge the Ministerio de Ciencia e Innovación-Agencia Estatal de Investigación through the projects PID2021-126235OB-C33 and TED2021-129555B-I00. Authors also thank the Generalitat Valenciana for CIAICO/2021/094, CIGRIS/2022/198 and for the financial support (CIACIF/2021/010).

Appendix A. Supplementary data

Supplementary data to this article can be found online at https://doi.org/10.1016/j.ceramint.2023.05.227.

References

[1] P. Dias, A. Vilanova, T. Lopes, L. Andrade, A. Mendes, Extremely stable bare hematite photoanode for solar water splitting, Nano Energy 23 (2016) 70–79.
[2] R. Li, Latest progress in hydrogen production from solar water splitting via photocatalysis, photoelectrochemical, and photovoltaic-photoelectrochemical solutions, Chin. J. Catal. 38 (2017) 5–12.
[3] H. Ahmad, S. Kamarudin, L.J. Minggu, M. Kassim, Hydrogen from photo-catalytic water splitting process: a review, Renew. Sustain. Energy Rev. 43 (2015) 599–610.
[4] A.A. Ismail, D.W. Bahnemann, Photochemical splitting of water for hydrogen production by photocatalysis: a review, Sol. Energy Mater. Sol. Cells 128 (2014) 85–101.
[5] N. Sahrin, R. Nawaz, F. Chong, S. Lee, M. Wirzal, Current Perspectives of Anodized TiO Nanotubes towards Photodegradation of Formaldehyde: A Short Review, vol. 22, Environmental Technology & Innovation, 2021, 101418.
[6] R.K. Nath, M.F.M. Zain, M. Jamil, An Environment-Friendly Solution for Indoor Aire Purification by Using Renewable Photocatalysts in Concrete: A Review, vol. 67, Renewable Sustainable Energy Rev, 2016, pp. 1184–1194.
[7] Y. Fu, A. Mo, A review on the electrochemically self-organized titania nanotube arrays: synthesis, modifications, and biomedical applications, Nanoscale Res. Lett. 13 (2018) 21.
[8] P. Roy, S. Berger, P. Schmuki, TiO_2 nanotubes: synthesis and applications, Angew. Chem. 50 (2011) 2904–2939.
[9] R.K. Karn, O. N Srivastava, On the synthesis of nanostructured TiO_2 anatase phase and the development of the photoelectrochemical solar cell, Int. J. Hydrogen Energy 24 (1999) 27–35.
[10] M. Nischk, P. Mazierski, Z. Wei, K. Siuzdak, N.A. Kouame, E. Kowalska, H. Remita, A. Zaleska-Medynska, Enhanced photocatalytic, electrochemical and photoelectrochemical properties of TiO_2 nanotubes arrays modified with Cu, AgCu and Bi nanoparticles obtained via radiolytic reduction, Appl. Surf. Sci. 387 (2016) 89–102.
[11] Y. Xia, P.S.Y. Yang, Y. Wu, B. Mayers, B. Gates, Y. Yin, F. Kim, H. Yan, One-dimensional nanostructures: synthesis, characterization, and applications, Adv. Mater. 15 (2003) 353–389.
[12] M. Asserpouf-Dezfuly, C. Vlachos, E.H. Andrews, Oxide morphology and adhesive bonding on titanium surfaces, J. Mater. Sci. 19 (1984) 3626–3639.
[13] V. Zwilling, E. Darque-Ceretti, A. Boutry-Forveille, D. David, M.Y. Perrin, M. Aucouturier, Structure and physicochemistry of anodic oxide films on titanium and TA6V alloy, Surf. Interface Anal. 27 (1999) 629–637.
[14] H. Wender, A.F. Feil, L.B. Diaz, C.S. Ribeiro, G.J. Machado, P. Migowski, D. E. Weibel, J. Dupont, S.R. Teixeira, Self-organized TiO_2 nanotube arrays: synthesis by anodization in an ionic liquid and assessment of photocatalytic properties, ACS Appl. Mater. Interfaces 3 (2011) 1359–1365.
[15] H.E. Prakasam, K. Shankar, M. Paulose, O.K. Varghese, C.A. Grimes, A new benchmark for TiO_2 nanotube array growth by anodization, J. Phys. Chem. C 111 (2007) 7235–7241.
[16] J.M. Macak, H. Tsuchiya, L. Taveira, S. Aldabergerova, P. Schmuki, Smooth anodic TiO_2 nanotubes, Angew. Chem. Int. Ed. 44 (2005) 7463–7746.
[17] S.P. Albu, A. Ghicov, J.M. Macak, P. Schmuki, 250 μm long anodic TiO_2 nanotubes with hexagonal self-ordering, Phys. Status Solidi Rapid Res. Lett. 1 (2007) R65–R67.
[18] M. Duerinck, Preparation of Ionic Liquids and Deep Eutectic Solvents for the Chemical Valorization of End-Of-Life Polylactide, Universitat de Valéncia, Valencia, 2020.
[19] A. Jordan, N. Gathergood, Biodegradation of ionic liquids - a critical review, Chem. Soc. Rev. 44 (2015) 8200–8237.
[20] B. Peric, J. Sierra, E. Martí, R. Cruañas, M.A. Garau, J. Arning, U. Bottin-Weber, S. Stolte, (Eco)toxicity and biodegradability of selected protic and aprotic ionic liquids, J. Hazard Mater. 261 (2013) 99–105.
[21] I. Paramasivam, J.M. Macak, T. Selvam, P. Schmuki, Electrochemical synthesis of self-organized TiO_2 nanotubular structures using an ionic liquid (BMIM-BF_4), Electrochim. Acta 54 (2008) 643–648.
[22] M.H. Dokoohaki, F. Mohammadpour, A.R. Zolghadr, New insight into electrosynthesis of ordered TiO_2 nanotubes in EG-based electrolyte solutions: combined experimental and computational assessment, Phys. Chem. Chem. Phys. 22 (2020) 22719–22727.
[23] H. Li, J. Qu, Q. Cui, H. Xu, H. Luo, M. Chi, R.A. Meisner, W. Wang, S. Dai, TiO_2 nanotube arrays grown in ionic liquids: high-efficiency in photocatalysis and pore-widening, J. Mater. Chem. 21 (2011) 9487–9490.
[24] Y. Yu, Y. Jiang, M. Tian, L. Yang, H. Yan, S. Sheng, N-doped TiO_2 nanotube arrays: synthesis by anodization in an ionic liquid ([BMIM]BF_4) and assessment of photocatalytic property, Rare Met. Mater. Eng. 45 (2016) 561–566.
[25] P. Mazierski, J. Łuczakb, W. Lisowskic, M.J. Winiarskid, T. Klimczukd, A. Zaleska-Medynskaa, The ILs-assisted electrochemical synthesis of TiO_2 nanotubes: the effect of ionic liquids on morphology and photoactivity, Appl. Catal. B Environ. 214 (2017) 100–113.
[26] A. Pancielejko, P. Mazierski, W. Lisowski, A. Zaleska-Medynska, J. Łuczak, Ordered TiO_2 nanotubes with improved photoactivity through self-organizing anodization with the addition of an ionic liquid: effects of the preparation conditions, ACS Sustainable Chem. Eng. 7 (2019) 15585–15596.
[27] A. Pancielejko, P. Mazierski, W. Lisowski, A. Zaleska-Medynska, K. Kosek, J. Łuczak, Facile Formation of self-organized TiO_2 nanotubes in electrolyte containing ionic liquid-ethylammonium nitrate and their remarkable photocatalytic properties, ACS Sustainable Chem. Eng. 6 (2018) 14510–14522.
[28] S.M. Hosseini, A. Hosseinian, S. Aparicio, An experimental and theoretical study om 2-hydroxyethylammonium acetate ionic liquid, J. Mol. Liq. 284 (2019) 271–281.
[29] S. Ghahramani, F. Yousefi, S.M. Hosseini, S. Aparicio, High pressure behavior of 2-hydroxyethylammonium acetate ionic liquid: experiment and molecular dynamics, J. Supercrit. Fluids 155 (2020), 104664.
[30] E.G.A. Rocha, T.C. Pin, S.C. Rabelo, A.C. Costa, Evaluation of the use of protic ionic liquids on biomass fractionation, Fuel 209 (2017) 145–154.
[31] R. Parra, M.S. Góes, M.S. Castro, E. Longo, P.R. Bueno, J.A. Varela, Reaction patwhay to the synthesis of anatase via the chemical modification of titanium isopropoxide with acetic acid, Chem. Mater. 20 (2008) 143–150.
[32] R.W. Parry, Química. Fundamentos Experimentales, Reverte, Barcelona, 1973.
[33] M. Nischk, P. Mazierski, M. Gazda, A. Zaleska, Ordered TiO_2 nanotubes: the effect of preparation parameters on the photocatalytic activity in air purification process, Appl. Catal. B Environ. 144 (2014) 674–685.
[34] K. Indira, S. Ningshen, U. Kamachi Mudali, N. Rajendran, Effect of anodization parameters on the structural morphology of titanium in fluoride containing electrolytes, Mater. Char. 71 (2012) 58–65.
[35] J.M. Macak, H. Tsuchiya, A. Ghicov, K. Yasuda, R. Hahn, S. Bauer, P. Schmuki, TiO_2 nanotubes: self-organized electrochemical formation, properties and applications, Curr. Opin. Solid State Mater. Sci. 11 (2007) 3–18.
[36] J.M. Macak, P. Schmuki, Anodic growth of self-organized anodic TiO_2 nanotubes in viscous electrolytes, Electrochim. Acta 52 (2006) 1258–1264.
[37] G. Zu, H. Li, S. Liu, D. Li, J. Wang, J. Zhao, High efficient mass determination of TiO_2 nanotube arrays and its application in lithium-ion batteries, Sustainable Materials and Techonologies 18 (2018), e00079.
[38] R. Hatel, M. Baitoul, Nanostructured Tungsten Trioxide (WO_3): synthesis, structural and morphological investigations, J. Phys. Conf. 1292 (2019), 012014.
[39] G. Roselló-Márquez, R.M. Fernández-Domene, J. García-Antón, Organophosphorus pesticides (chlorfenvinphos, phosmet and fenamiphos) photoelectrodegradation by using WO_3 nanostructures as photoanode, J. Electroanal. Chem. 894 (2021), 115366.
[40] Y. Guo, X. Quan, N. Lu, H. Zhao, S. Chen, High photocatalytic capability of self-assembled nanoporous WO_3 with preferential orientation of (002) planes, Environ. Sci. Technol. 42 (2007) 4422–4427.
[41] Z.F. Huang, J. Song, L. Pan, X. Zhang, L. Wang, J.J. Zou, Tungsten oxides for photocatalysis, electrochemistry, and phototherapy, Adv. Mater. 27 (2015) 5309–5327.

[42] D.P. Oyarzún, R. Córdova, O.E. Linarez, E. Muñoz, R. Henríquez, M. López, H. Gómez, Morphological, electrochemical and photoelectrochemical characterization of nanotubular TiO_2 synthetized electrochemically from different electrolytes, J. Solid State Electrochem. 15 (2011) 2265–2275.
[43] P. Acevedo-Peña, I. González, TiO_2 nanotubes formed in aqueous media: relationship between morphology, electrochemical properties and photoelectrochemical performance for water oxidation, Journal of the Electrochemial Society 160 (2013) H454–H458.
[44] T. Zhu, M. Chong, Y. Phuan, E. Chan, Electrochemically synthesized tungsten trioxide nanostructures for photoelectrochemical water splitting: influence of heat treatment on physicochemical properties, photocurrent densities and electron shutting, Colloids Surf. A Physicochem. Eng. Asp. 484 (2015) 297–303.
[45] L. Li, X. Zhao, D. Pan, G. Li, Nanotube array-like WO_3/W photoanode fabricated by electrochemical anodization for photoelectrocatalytic overall water splitting, Chin. J. Catal. 38 (2018) 2132–2140.
[46] D. Bonham, A mathematical model for the influence of deep-level electronic states on photoelectrochemical impedance spectroscopy, J. Electrochem. Soc. 139 (1992) 127–137.
[47] C.W. Chu, New ordered phases of slightly reduced rutile and their sharp dielectric absorptions at low temperature, Phys. Rev. B 1 (1970) 4700–4708.
[48] J. Borràs-Ferris, R. Sánchez-Tovar, E. Blasco-Tamarit, R. Fernández-Domene, J. García-Antón, Effect of Reynolds number and lithium cation insertion on titanium anodization, Electrochim. Acta 196 (2016) 24–32.
[49] G.L. Martínez, Nanoestructuras de TiO_2 de baja dimensionalidad para la obtención fotocatalítica de hidrógeno, Universitat Politècnica de Catalunya, Barcelona, 2019.
[50] V. Vega, Fabricación de membranas nanoporosas de alúmina mediante técnicas electroquímicas, Universidad de Oviedo, Asturias, 2012.
[51] P. Makula, M. Pacia, W. Macyk, How to correctly determine the band gap energy of modified semiconductor photocatalysts based on UV-vis spectra, J. Phys. Chem. Lett. 9 (2018) 6814–6817.
[52] S. Valencia, J.M. Marín, G. Restrepo, Study of the bandgap of synthesized titanium dioxide nanoparticules using the sol-gel method and a hydrothermal treatment, Open Mater. Sci. J. 4 (2010) 9–14.
[53] M. Ikram, M. Rashid, A. Haider, S. Naz, J. Haider, A. Raza, M. Ansar, M. Uddin, N. Ali, S. Ahmed, M. Imran, S. Dilpazir, Q. Khan, M. Maqbool, A review of photocatalytic characterization, and environmental cleaning, of metal oxide nanostructured materials, Sustainable Materials and Technologies 30 (2021) 1–42.
[54] E. Blasco-Tamarit, B. Solsona, R. Sánchez-Tovar, D. García-García, R. Fernández-Domene, García-Antón, J, Influence of annealing atmosphere on photoelectrochemical response of TiO_2 nanotubes anodized under controlled hydrodynamic conditions, J. Electroanal. Chem. 897 (2021) 115579–115592.